Elsevier Editorial System(tm) for Applied Catalysis B: Environmental
Manuscript Draft

Manuscript Number: APCATB-D-08-00179R1

Title: Development of an S-doped titania nanotube (TNT) site-selectively loaded with iron(III) oxide and its photocatalytic activities.

Article Type: Full Length Article

Keywords: photocatalysts; TiO2 nanotube; visible light; S-doped TNT; oxidation of acetaldehyde; site-selective loading of iron oxide (III)

Corresponding Author: Teruhisa Ohno,

Corresponding Author's Institution:

First Author: Kazumoto Nishijima

Order of Authors: Kazumoto Nishijima; Yuichi Fujisawa; Naoya Murakami; Toshiki Tsubota; Teruhisa Ohno

Development of an S-doped titania nanotube (TNT) site-selectively loaded with iron(III) oxide and its photocatalytic activities.

Kazumoto Nishijima, Yuichi Fujisawa, Naoya Murakami, Toshiki Tsubota and Teruhisa Ohno

Department of Applied Chemistry, Faculty of Engineering, Kyushu Institute of Technology,

1-1 Sensuicho, Tobata, Kitakyushu 804-8550, Japan

Corresponding author:

Teruhisa Ohno

Tel.&FAX +81-93-884-3318

E-mail: tohno@che.kyutech.ac.jp

Abstract

We investigated an S-doped titania nanotube (TNT) loaded with Fe_2O_3 nanoparticles in order to improve photocatalytic activity of S-doped TNT under visible light irradiation. S-doped TNT was successfully prepared using the solid-phase method at 350 °C under aerated conditions. S-doped TNT showed photoabsorption in the 400 nm to 500 nm visible light region and showed photocatalytic activity for oxidation of acetaldehyde under visible light irradiation. Loading of Fe_2O_3 on S-doped TNT remarkably improved the photocatalytic activity of S-doped TNT. PA spectra measurement, which was performed in order to elucidate the mechanism of activity improvement, showed that the efficiency of charge separation between photoexcited electrons and holes was improved because the electrons were trapped by Fe_2O_3. Enhancement of photocatalytic activity was strongly dependent on the site of Fe_2O_3 nanoparticles loaded on TNT. PA spectra measurement showed that the photoexcited electrons transferred to Fe_2O_3 from S-doped TNT under UV light irradiation or to S-doped TNT from Fe_2O_3 under visible light irradiation.

Keywords: photocatalysts; TiO_2 nanotube; visible light; S-doped TNT; oxidation of acetaldehyde; site-selective loading of iron oxide (III)

1. Introduction

Titanium(IV) oxide (TiO_2) has been used to reduce environmental pollution and destruction on a global scale due to its excellent photocatalytic activities, such as a high level of oxidation ability and super-hydrophilicity [1]. In addition, TiO_2 has been generically used as a catalyst because of its optical and electronic properties, low cost, high level of photocatalytic activity, chemical stability and non-toxicity [2].

Nanosized materials derived from TiO_2 have been extensively investigated for various applications, including solar cells/batteries, electrode materials and photocatalysis, owing to their unique chemical and physical behaviors [3-6]. Moreover, since the discovery of a carbon nanotube [7], there have been many studies on one-dimensional nanostructures, such as nanotubes, nanorods and nanowires. TiO_2-based nanotubes with a highly specific surface area, ion-changeable ability and photocatalytic ability have been considered for extensive applications [5, 6, 8]. However,

unfortunately, this nanotube itself does not have a high level of photocatalytic ability due to its low crystallinity. In addition, TNT and TiO_2 absorb only UV light because their band gap energy is too high. In order to improve its ability of absorption, visible light sanitization of TNT has been studied extensively. In the case of development of visible-light sensitive TiO_2, TiO_2 is doped with S atoms, N atoms or C atoms [9-17]. When these atoms are doped into TiO_2, they create impurity levels between the conduction band and valence band, resulting in a decrease in band gap energy. However, impurity levels also act as recombination centers, resulting in a decrease in photocatalytic activity under UV light irraidation. Therefore, it is necessary to prevent recombination between photoexcited electrons and holes in order to improve photocatalytic activity. In our previous study, we successfully developed visible-light sensitive TiO_2 that showed a high level of photocatalytic activity by loading of Fe_2O_3 on the TiO_2 surface [12].

In this study, we developed an S-doped TNT using the solid-phase method with heat treatment at a temperature lower than 350 °C because thermostability of TNT is low compared to that of conventional spherical-shape of TiO_2 particles. The S-doped

TNT showed photocatalytic activity for oxidation of acetaldehyde under visible light irradiation. The S-doped TNT was site-selectively loaded with Fe_2O_3. Photocatalytic activities of S-doped TNT powders loaded with Fe_2O_3 varied depending on site of the Fe_2O_3 loading.

2. Experimentals

2.1. Materials and instruments

TNT was kindly supplied by Catalysts & Chemicals Ind. Co., Ltd. The BET relative surface areas of pure TNT powder and S-doped TNT powder by calcination at 350 °C were 114.0 $m^2\ g^{-1}$ and 101.5 $m^2\ g^{-1}$, respectively. Thiourea and iron(III) nitrate nonahydrate were obtained from Wako Pure Chemical Industry. Acetaldehyde was obtained from Aldrich Chemical Company, Inc. Other chemicals were obtained from commercial sources as guaranteed reagents and used without further purification. The crystal structures of pure TNT and S-doped TNT were determined from X-ray diffraction (XRD) patterns measured by using an X-ray diffractometer (Philips, X'Pert-MRD) with a Cu target Kα-ray ($\lambda = 1.5405\times10^{-1}$ nm). The relative surface areas

of the powders were determined by N_2 adsorption/desorption isotherm analysis (BET method). The measurements were performed using a Micromeritics FlowSorb II 2300. TEM observations were performed using a HITACHI H-9000NAR. The diffuse reflection spectra were measured using a Shimadzu UV-2500PC spectrophotometer. X-ray photoelectron spectra (XPS) of the powders were measured using a JEOL JPS90SX photoelectron spectrometer with an Mg Kα source (1253.6 eV). The shift of binding energy due to relative surface charging was corrected using the C 1s level at 284.6 eV as an internal standard. The XPS peaks were assumed to have Gaussian line shapes and were resolved into components by a non-linear least-squares procedure after proper subtraction of the baseline.

2.2. Preparation of S-doped TNT and loading of Fe_2O_3 on S-doped TNT

S-doped TNT was synthesized by previously reported methods except calcination temperature [9-12]. When calcination temperature for doping S atoms into TNT was higher than 350 °C, the TNT structure was completely destroyed. Therefore, calcination temperature for doping was maintained to 350 °C.

In order to improve the photocatalytic activity of S-doped TNT, Fe_2O_3 was loaded on the inside surface and/or outside surface of S-doped TNT. The procedure for preparing S-doped TNT loaded with Fe_2O_3 nanoparticles is as follows. An appropriate amount of iron(III) nitrate nonahydrate was dissolved in 300 mL deionized water. Three g of S-doped TNT was suspended in a $Fe(NO_3)_3$ aqueous solution, and the solution was stirred vigorously for 2 hours. After filtration of the solution, the amount of Fe^{3+} ions that remained in the solution was determined by a UV absorption spectrum in order to estimate the amount of Fe_2O_3 loaded on S-doped TNT. The residue was washed with deionized water several times until pH of the filtrate was neutralized. The powders were dried under reduced pressure at 60 °C for 3 hours. The sample loaded with Fe_2O_3 particles on the inside and outside surfaces of S-doped TNT is abbreviated as Fe-STNT-i/o.

Fe_2O_3 nanoparticles were loaded on the inside or outside surface of S-doped TNT as follows. First, S-doped TNT loaded with Fe_2O_3 particles on the inside surface of the nanotube was prepared as follows. Fe_2O_3 particles were adsorbed on the inside and outside surfaces of TNT by Fe^{3+} ion aqueous solution impregnation as discribed

previously. Then in order to remove Fe_2O_3 particles on the outside surface of TNT, Fe_2O_3-loaded TNT was washed with HCl aqueous solution. After washing with HCl aqueous solution, the TNT was washed with deionized water several times and dried under reduced pressure at 60 °C for 3 hours. The sample loaded with Fe_2O_3 particles on the inside surface of S-doped TNT is abbreviated as Fe-STNT-i.

Loading of Fe_2O_3 particles on the outside surface of TNT was performed as follows. TNT powder was spread evenly on the bottom of a glass dish and sprayed with Fe^{3+} ion aqueous solution and then allowed to dry by itself. Then the TNT powder was stirred. This treatment was performed several times. The sample loaded with Fe_2O_3 particles on the outside surface of S-doped TNT is abbreviated as Fe-STNT-o. Amounts of Fe_2O_3 loaded on Fe-STNT-i/o, Fe-STNT-i and Fe-STNT-o were shown by ICP measurements to be 0.98 wt%, 0.18 wt% and 0.95 wt%, respectively.

2.3. Photocatalytic degradation of acetaldehyde in gas phase

Photocatalytic activities of the TNT powders were evaluated by measuring the change in concentrations of acetaldehyde and CO_2 evolved by oxidation as a function of

irradiation time. A Tedlar bag (AS ONE Co. Ltd.) was used as the photo-reactor vessel with a volume of 125 cm^3. One hundred mg of TNT powder was spread evenly on the bottom of a glass dish (area: 9.6 cm^2 = irradiation area), and the glass dish was placed in the reaction vessel as described above.

Five hundred ppm of acetaldehyde was prepared in the vessel by injection of saturated gaseous acetaldehyde. The irradiations were conducted at room temperature after equilibrium between the gaseous and adsorbed acetaldehyde had been reached, which was ascertained by monitoring the concentration by a gas chromatograph about every 30 min. A 500 W Xe lamp (USHIO Co. Ltd., SX-UI501XQ) was used as a light source. UV-35 and L-42 cutoff filters were used in order to adjust wavelength of incident light to longer than 350 nm and 420 nm, respectively. Fine stainless meshes were used as neutral density filters to adjust the irradiation intensity (12.7 mW cm^{-2}). After starting the irradiation, the decrease in acetaldehyde concentration was measured using a gas chromatograph (Shimadzu Model GC-8A, FID detector) equipped with a PEG-20M 20% Celite 545 packed glass column and using CR-8A CHROMATOPAC for data processing. At the same time, the amount of gaseous carbon dioxide evolved

was analyzed using a gas chromatograph (Shimadzu Model GC-9A, FID detector) equipped with a TCP 20% Uniport R packed column and a methanizer (GL Sciences, MT-221) operated at a temperature of 375°C and using CR-8A CHROMATOPAC for data processing.

2.4. Photoacoustic spectroscopic analysis

In order to analyze the role of Fe_2O_3 nanoparticles loaded on the TNT, we measured the photoacoustic spectra (PA spectra) of a pure TNT sample and of S-doped TNT samples. PA spectra were measured as previously reported [18,19]. A flow-type PA cell in which the atmosphere was controlled by the flow of 2-propanol vapor containing nitrogen was used for time-resolved measurements. TNT powder was placed in the cell. The 2-propanol-nitrogen gas was injected into the PA cell for 30 minutes. TNT powder was photoirradiated using light-emitting diodes (Nichia NCCU033, Luxeon LXHL-NB98) emitting light at 365 nm and at 470 nm for excitation of the TNT. An LED (Luxeon LXHL-ND98) emitting light at 625 nm as a probe light source was used, and its output intensity was modulated by a digital function generator (NF DF1905) at

80 Hz. The PA signal acquired by a condenser microphone buried in the cell was amplified and monitored by a digital lock-in amplifier (NF LI 5640).

3. Results and discussion

3.1. Characterization of S-doped TNT

Figure 1 shows diffuse reflectance spectra of pure TNT, S-doped TNT and S-doped TNT loaded with Fe_2O_3 particles. S-doped TNT showed photoabsorption in the 390 nm to 500 nm visible light region. S atoms doped into TiO_2 bulk formed impurity levels above the valence band, resulting in a decrease in band gap energy [10]. After loading of Fe_2O_3 particles on S-doped TNT, the photoabsorption of S-doped TNT in the visible light region increased slightly because the incident visible light was absorbed by Fe_2O_3 loaded on S-doped TNT. Photoabsorption in the visible light region of Fe-STNT-i was slightly lower than that of Fe-STNT-i/o and Fe-STNT-o as shown in Figure 1. The incident visible light was not absorbed by Fe_2O_3 because Fe_2O_3 was loaded on the inside surface of S-doped TNT.

Figure 2 shows an S2p spectrum of S-doped TNT. Two peaks were observed

around 162 eV and around 168 eV as shown in the figure. The peak at around 168 eV was resolved into two peaks centered at 168.5 eV and 170.3 eV. A peak centered at 168.5 eV was assigned to S^{4+} cation substituted for Ti^{4+} cation [10]. A peak at 170.3 eV was assigned to SO_4^{2-} generated by thermal decomposition of thiourea [10]. On the other hand, peaks at around 162 eV were assigned to residual thiourea due to the low calcination temperature. The chemical state of Fe atoms adsorbed on S-doped TNT was assigned to Fe^{3+} by XPS spectra as shown in Figure 3.

Figure 4 shows XRD patterns of pure TNT and S-doped TNT. Peaks assigned to titanate ($H_2Ti_4O_9 \cdot H_2O$) phase were observed at 2θ = 24.3°, 28.5° and 49.5° in the XRD pattern of pure TNT [20]. After doping of S atoms under calcination at 350 °C, peaks assigned to anatase were observed at 2θ = 25.3°, 37.7°, 48.3° and more. These results indicated that the crystal phase was changed from titanate ($H_2Ti_4O_9 \cdot H_2O$) to anatase (TiO_2) by thermal treatment.

Figure 5 shows TEM images of pure TNT (Figure 5 (a)) and S-doped TNT (Figure 5 (b)). Structure of a nanotube was observed as shown in Figure 5 (a). The inner and outer diameters of pure TNT ranged from 4.3 nm to 5.7 nm and from 8.6 nm to 11.4

nm, respectively. The average inner diameter and average outer diameter of pure TNT were 5.0 nm and 10.2 nm, respectively. Figure 5 (b) shows that the structure of the nanotube was not destroyed after calcination at 350 °C. The inner and outer diameters of S-doped TNT ranged from 4.3 nm to 5.7 nm and from 8.6 nm to 11.4 nm, respectively. The average inner diameter and average outer diameter of S-doped TNT were 5.1 nm and 10.6 nm, respectively. After calcination, the inner diameter and outer diameter of nanotubes were not changed.

3.2. PA spectra of S-doped TNT loaded with Fe_2O_3 particles

In order to elucidate electron transfer, we performed photoacoustic (PA) analysis. PA intensity indicates that amount of Ti^{3+} ions generated by photoexcited electrons [18,19]. If the photoexcited electrons do not transfer to molecules such as O_2 molecules adsorbed on the surface of TiO_2, the electrons are trapped at Ti^{4+} sites in TiO_2 and reduce Ti^{4+} ions to Ti^{3+} ions in the bulk of TiO_2 or on the surface of TiO_2, resulting in an increase in PA intensity. In the case of TNT loaded with Fe_2O_3, PA intensity is expected to decrease compared with that in the case of pure TNT because photoexcited

electrons are efficiently trapped by Fe^{3+} in Fe_2O_3 on TNT.

Figure 6 (a) shows PA spectra of pure TNT, S-doped TNT and S-doped TNT loaded with Fe_2O_3 under incident light of center wavelength at 365 nm. PA intensity of S-doped TNT was stronger than that of pure TNT and increased with photoirradiation time. The amount of Ti^{3+} ions in the bulk of and on the surface of S-doped TNT was larger than that of Ti^{3+} ions in the bulk of and on the surface of pure TNT. The electron transfer from S-doped TNT to O_2 molecules was slower than that of pure TNT to O_2 molecules. PA intensities of S-doped TNT loaded with Fe_2O_3 decreased remarkably compared with that of S-doped TNT under UV light irradiation as shown in Figure 6 (a). The amount of Ti^{3+} ions in S-doped TNT was decreased by loading of Fe_2O_3. The photoexcited electrons were efficiently trapped by Fe_2O_3 on the surface of S-doped TNT as shown in Figure 7. The PA spectrum of Fe-STNT-i/o overlapped with that of Fe-STNT-i as shown in Figure 6 (a). The ability of electron trapping of Fe_2O_3 loaded on the inside surface of S-doped TNT was greater than that of Fe_2O_3 deposited on the outside surface of S-doped TNT as shown in Figure 7. Therefore, the PA intensity of Fe-STNT-o was higher than that of Fe-STNT-i and Fe-STNT-i/o. Fe-STNT-i efficiently

absorbed UV light compared to Fe-STNT-o because UV light did not reach the surface of Fe-STNT-o due to coverage of Fe_2O_3 on the outer side of S-doped TNT.

Figure 6 (b) shows PA spectra of pure TNT, S-doped TNT and S-doped TNT loaded with Fe_2O_3 under incident light of center wavelength at 470 nm. The PA spectrum of pure TNT was flat during continuous photoirradiation because pure TNT was not photoexcited under visible light. The PA intensity of S-doped TNT increased during continuous photoirradiation because S-doped TNT was photoexcited by visible light irradiation. The PA intensity of Fe-STNT-o was higher than that of S-doped TNT without Fe_2O_3 as shown in Figure 6 (b). This result suggested that the amount of Ti^{3+} ions in S-doped TNT increased during continuous photoirradiation. The photoexcited electrons generated in Fe_2O_3 loaded on the outside surface were injected into S-doped TNT and reduced Ti^{4+} to Ti^{3+} as shown in Figure 7. In addition, photoexcitation of Fe_2O_3 loaded on the outside surface of S-doped TNT occurred preferentially compared to that of S-doped TiO_2 under visible light irradiation. On the other hand, PA intensity of Fe-STNT-i was lower than that of S-doped TNT as shown in Figure 6 (b). The photoexcited electrons in S-doped TNT under visible light irradiation transferred to

Fe_2O_3 loaded on the inside surface of S-doped TNT, resulting in a decrease in the amount of Ti^{3+} ions. Thus, the directions of the electron transfer of Fe-STNT-i and Fe-STNT-o are thought to be opposite (Figure 7). The PA intensity of Fe-STNT-i/o was lower than that of the other samples. Fe_2O_3 loaded on the outside surface of S-doped TNT was photoexcited under visible light irradiation. The photoexcited electrons transferred to the conduction band of S-doped TNT, and then the photoexcited electrons were trapped by Fe_2O_3 loaded on the inside surface of S-doped TNT. The photoexcited electrons transferred smoothly to Fe_2O_3 loaded on the inside surface from Fe_2O_3 loaded on the outside surface as shown in Figure 7.

3.3. Photocatalytic activities of TNT with various treatments for acetaldehyde oxidation

The photocatalytic activities of photocatalysts were evaluated by photocatalytic oxidation of acetaldehyde in gas phase. Figure 8 shows the photocatalytic activities of pure TNT, S-doped TNT and S-doped TNT loaded with Fe_2O_3 for oxidation of acetaldehyde under incident light longer than 350 nm (Figure 8 (a)) and incident light longer than 420 nm (Figure 8 (b)). S-doped TNT showed a lower level of photocatalytic

activity for oxidation of acetaldehyde than did pure TNT under UV light irradiation as shown in Figure 8 (a). Impurity levels formed by S doping treatment above the valence band acted as recombination centers. The photocatalytic activity of S-doped TNT loaded with Fe_2O_3 was remarkably improved compared with that of S-doped TNT without Fe_2O_3 as shown in Figure 8 (a). PA measurement (Figure 6 (a)) showed that photoexcited electrons were trapped by Fe_2O_3 loaded on S-doped TNT and that the efficiency of charge separation was improved. However, the order of rates of CO_2 generation changed after 120 min of photoirradiation depending on the site of Fe_2O_3 deposition. From 0 min to 120 min of photoirradiation, the photocatalytic activities of Fe-STNT-i/o Fe-STNT-o and Fe-STNT-i decreased in that order. The lowest level of photocatalytic activity for Fe-STNT-i was thought to be due to the slow rate of diffusion of oxygen molecules into nanotubes. Recombination between electrons and holes proceeded because electrons accumulated at Fe_2O_3 particles. In the case of Fe-STNT-i/o and Fe-STNT-o, the electrons trapped by Fe_2O_3 transferred smoothly to oxygen molecules because O_2 molecules were supplied in large amounts to Fe_2O_3 particles due to loading on the outside surface of S-doped TNT. In addition, acetaldehyde is directly

oxidized to CO_2 with $^{\bullet}OH$ generated by reaction of Fe^{2+} and H_2O_2 [21,22]. The rate of the direct oxidation of acetaldehyde to evolve CO_2 is very fast [21]. Hydroxyl radical was generated on the outside surface of S-doped TNT in the case of Fe-STNT-i/o and Fe-STNT-o. Therefore, acetaldehyde was easily oxidized with hydroxyl radical on Fe-STNT-i/o and F-STNT-o, resulting in an increase in photocatalytic activity compared with that of Fe-STNT-i.

On the other hand, the order of photocatalytic activities was Fe-STNT-i > Fe-STNT-o > Fe-STNT-i/o from 120 min to 480 min of photoirradiation. Especially, the rate of CO_2 evolved on Fe-STNT-i/o became slow after 120 min of photoirradiation as shown in Figure 8 (a). Figure 9 shows IR spectra of Fe-STNT-i/o during oxidation of acetaldehyde at the 60 min and 120 min of reaction time. Two peaks assigned to acetic acid were observed at 1540 cm^{-1} and 1440 cm^{-1} [21]. This result suggested that acetic acid was generated by oxidation of acetaldehyde. Therefore, oxidation of acetic acid proceeded during photoirradiation from 120 min to 480 min. The oxidation of acetaldehyde consisted of two routes which are the direct oxidation of acetaldehyde to generate CO_2 and evolution of CO_2 via oxidation of acetic acid (formula (1) and (2))

[21,22].

$$2CH_3CHO + 2^{\bullet}OH + O_2 \rightarrow 2CH_3^{\bullet} + 2CO_2 + 2H_2O \quad (1)$$

$$CH_3COOH + h^+ \rightarrow CO_2 + CH_3^{\bullet} + H^+ \quad (2)$$

When acetic acid was generated on TiO_2 loaded with Fe_2O_3, the evolution of CO_2 became slow because oxidation of acetic acid was difficult compared to the direct oxidation of acetaldehyde, resulting in a decrease in rate of CO_2 evolved [21]. The efficiency of charge separation is important for oxidation of acetic acid since acetic acid has been shown to be mainly oxidized with holes [23,24].

PA spectra showed that the efficiency of charge separation of Fe-STNT-i was highest among the samples loaded with Fe_2O_3 (Figure 6 (a)), and the active sites on the surface of Fe-STNT-i were not covered with Fe_2O_3 particles. Therefore, Fe-STNT-i showed the highest level of photocatalytic activity in photoirradiation longer than 120 min. In the case of Fe-STNT-i/o and Fe-STNT-o, Fe_2O_3 particles loaded on the outside surface were thought to act as recombination centers, resulting in a decrease in

photocatalytic activities. Oxidation of acetic acid proceeded on the outside surface of S-doped TNT. Photoexcited electrons also transferred to the outside surface of S-doped TNT. Therefore, recombination between electrons and holes was thought to proceed.

S-doped TNT showed photocatalytic activity under visible light irradiation longer than 420 nm, but pure TNT did not (Figure 8 (b)). The photocatalytic activity level of S-doped TNT loaded with Fe_2O_3 was higher than that of S-doped TNT without Fe_2O_3 under visible light irradiation (Figure 8 (b)). Fe-STNT-o showed the highest level of photocatalytic activity. Fe_2O_3 loaded on the outside surface of S-doped TNT was photoexcited under visible light irradiation. PA analysis showed that the photoexcited electrons in the bulk of Fe_2O_3 transferred to the conduction band of S-doped TNT under visible light irradiation (Figure 6 (b)). Acetaldehyde was oxidized by the holes generated by photoexcitation of Fe_2O_3. Hydroxyl radical generated by O_2 reduced by electrons in conduction band of S-doped TNT also oxidized acetaldehyde [21,22]. On the other hand, the photocatalytic activity of Fe-STNT-i was similar to that of S-doped TNT. In the case of Fe-STNT-i, Fe_2O_3 was photoexcited by visible light which penetrated the wall of S-doped TNT. However, acetaldehyde was hardly oxidized by the

holes in Fe_2O_3 loaded on the inside surface of S-doped TNT because the diffusion rate of acetaldehyde into S-doped TNT was thought to be quite slow. Fe_2O_3 loaded on the inside surface of S-doped TNT trapped the photoexcited electrons in the conduction band of S-doped TNT, resulting in a slight increase in photocatalytic activity. However, Fe_2O_3 did not work efficiently because few photoexcited electrons and holes were generated on S-doped TNT under visible light irradiation. The apparent quantum yields were estimated from amount of CO_2 evolved after 120 min of photoirradiation. The apparent quantum yields of Fe-STNT-i/o, Fe-STNT-i and Fe-STNT-o were 9.0, 5.7 and 4.9, respectively, under incident light at 385 nm. Under incident light at 420 nm, the apparent quantum yields of Fe-STNT-i/o, Fe-STNT-i and Fe-STNT-o were 1.8, 1.8 and 2.2, respectively.

4. Conclusion

We successfully developed visible light-sensitive TNT by doping S atoms. Diffuse reflectance spectra showed that the absorption edge of S-doped TNT was shifted to a longer wavelength. Photoabsorption of S-doped TNT in the visible light

region increased with increase in the amount of Fe_2O_3 loaded on S-doped TNT due to absorption of Fe_2O_3. S-doped TNT showed a photocatalytic activity for oxidation of acetaldehyde under visible light irradiation, while pure TNT did not show such photocatalytic activity. Photocatalytic activity of S-doped TNT loaded with Fe_2O_3 nanoparticles was remarkably improved. Under UV light irradiation at wavelengths longer than 350 nm, Fe-STNT-i showed the highest level of photocatalytic activity because Fe_2O_3 loaded on S-doped TNT trapped the photoexcited electrons, resulting in an increase in efficiency of charge separation. On the other hand, under visible light irradiation at wavelengths longer than 420 nm, Fe-STNT-o showed the highest level of photocatalytic activity because the photoexcited electrons in Fe_2O_3 loaded on S-doped TNT transferred to S-doped TNT and the holes in Fe_2O_3 oxidized acetaldehyde.

Acknowledgement

This work was supported by a Grant-in-Aid for Scientific Research from the Ministry of Education, Culture, Science, and Technology (MEXT), Japan and Nissan Science Foundation. This work was partly supported by a grant of Knowledge Cluster

Initiative implemented by the Ministry of Education, Culture, Sports, Science and Technology (MEXT).

References

[1] M. R. Hoffman, S. T. Martin, W. Choi, D. W. Bahnemann, Chem. Rev. 95 (1995) 69.

[2] A. Fujishima, T. N. Rao, D. A. Truk, J. Photochem. Photobiol. C: Photochem. Rev. 1 (2000) 1.

[3] S. Uchida, R. Chiba, M. Tomiha, N. Masaki, M. Shirai, Electrochem. 70 (2002) 418.

[4] A. R. Armstrong, G. Armstrong, Angew. Chem. Int. Ed. 43 (2004) 2286.

[5] A. Nakahira, W. Kato, M. Tamai, T. Isshiki, K. Nishio, H. Aritani, J. Mater. Sci. 39 (2004) 4239.

[6] H. Tokudome, M. Miyauchi, Chem. Lett. 33 (2004) 1108.

[7] S. Iijima, Nature 354 (1991) 56.

[8] X. Sun, Y. Li, Chem. Eur. J. 9 (2003) 2229.

[9] T. Ohno, T. Mitsui, M. Matsumura, Chem. Lett 32 (2003) 364.

[10] T. Ohno, M. Akiyoshi, T. Umebayashi, K. Asai, T. Mitsui, M. Matsumura, Appl. Catal. A., General 265 (2004) 115.

[11] T. Ohno, T. Tsubota, M. Toyofuku, R. Inaba, Catal. Lett. 98 (2004) 255.

[12] T. Ohno, Z. Miyamoto, K. Nishijima, H. Kanemitsu, and F. Xueyuan, Appl. Catal. A: General 302 (2006) 62.

[13] S. Sato, Chem. Phys. Lett., 123 (1986) 126.

[14] R. Asahi, T. Morikawa, T. Ohwaki, K. Aoki, and Y. Taga, Science 295 (2002) 627.

[15] Y. Nosaka, M. Matsushita, J. Nishino, and AY Nosaka, Science and Technology of Advanced Materials 6 (2005) 1468.

[16] H. Irie, Y. Watanabe, and K. Hashimoto, Chemistry Letter 32 (2003) 772-773.

[17] S. Sakthivel and H. Kisch, Angewandte Chemie-International Edition 42 (2003) 4908.

[18] N. Murakami, O. O. P. Mahaney, T. Torimoto, and B. Ohtani, Chemical Physics Letters 426 (2006) 204-208.

[19] N. Murakami, O. O. P. Mahaney, R. Abe, T. Torimoto, and B. Ohtani, The Journal of Physical Chemistry C 111 (2007) 11927-11935.

[20] A. Nakahira, W. Kato, M. Tamai, T. Isshiki, K. Nishio, and H. Aritani, Journal of

Materials Science 39 (2004) 4239-4245.

[21] K. Nishijima, B. Ohtani, X.Yan, N. Murakami, T. Kamai, T. Chiyoya, and T. Ohno, Chemical Physics 339 (2007) 64-72.

[22] N. R. Nimlos, E. J. Wolfrum, M. L. Brewer, J. A. Fennell, and G. Binter, Environmental Science and Technology 30 (1996) 3102-3110.

[23] S. Sato, The Journal of Physical Chemistry 87 (1983) 3531-3537.

[24] Y. Nosaka, M. Kishimoto, and J. Nishino, The Journal of Physical Chemistry B 102 (1998) 10279-10283.

Figure captions

Figure 1 Diffuse reflectance spectra of pure TNT, S-doped TNT and S-doped TNT samples loaded with Fe_2O_3 particles (a) and magnified figure of Figure 1 (a) at the range between 0 and 0.4 in absorbance (b).

Figure 2 S 2p spectrum of S-doped TNT with calcinations at 350 °C.

Figure 3 Fe 2p spectra of Fe_2O_3, Fe-STNT-i/o, Fe-STNT-i and Fe-STNT-o.

Figure 4 XRD patterns of pure TNT without calcinations (a) and S-doped TNT with calcinations at 350 °C (b).

Figure 5 TEM images of pure TNT without calcinations (a) and S-doped TNT (b) with calcinations at 350 °C (b).

Figure 6 PA spectra of pure TNT, S-doped TNT, and S-doped TNT samples loaded with

Fe_2O_3 under incident light of center wavelength at 365 nm (a) or under incident light of center wavelength at 470 nm (b).

Figure 7 Mechanism of trapping of the photoexcited electrons by Fe_2O_3 loaded on S-doped TNT under UV light irradiation or under visible light irradiation.

Figure 8 Amount of evolved CO_2 by oxidation of acetaldehyde over pure TNT, S-doped TNT and S-doped TNT samples loaded with Fe_2O_3 as a function of photoirradiation time under UV light irradiation at wavelengths longer than 350 nm (a) or under visible light irradiation at wavelengths longer than 420 nm (b).

Figure 9 IR spectra of Fe-STNT-i/o after oxidation of acetaldehyde for 60 min and 120 min of photoirradiation under UV light irradiation at wavelengths longer than 350 nm.

figure 1

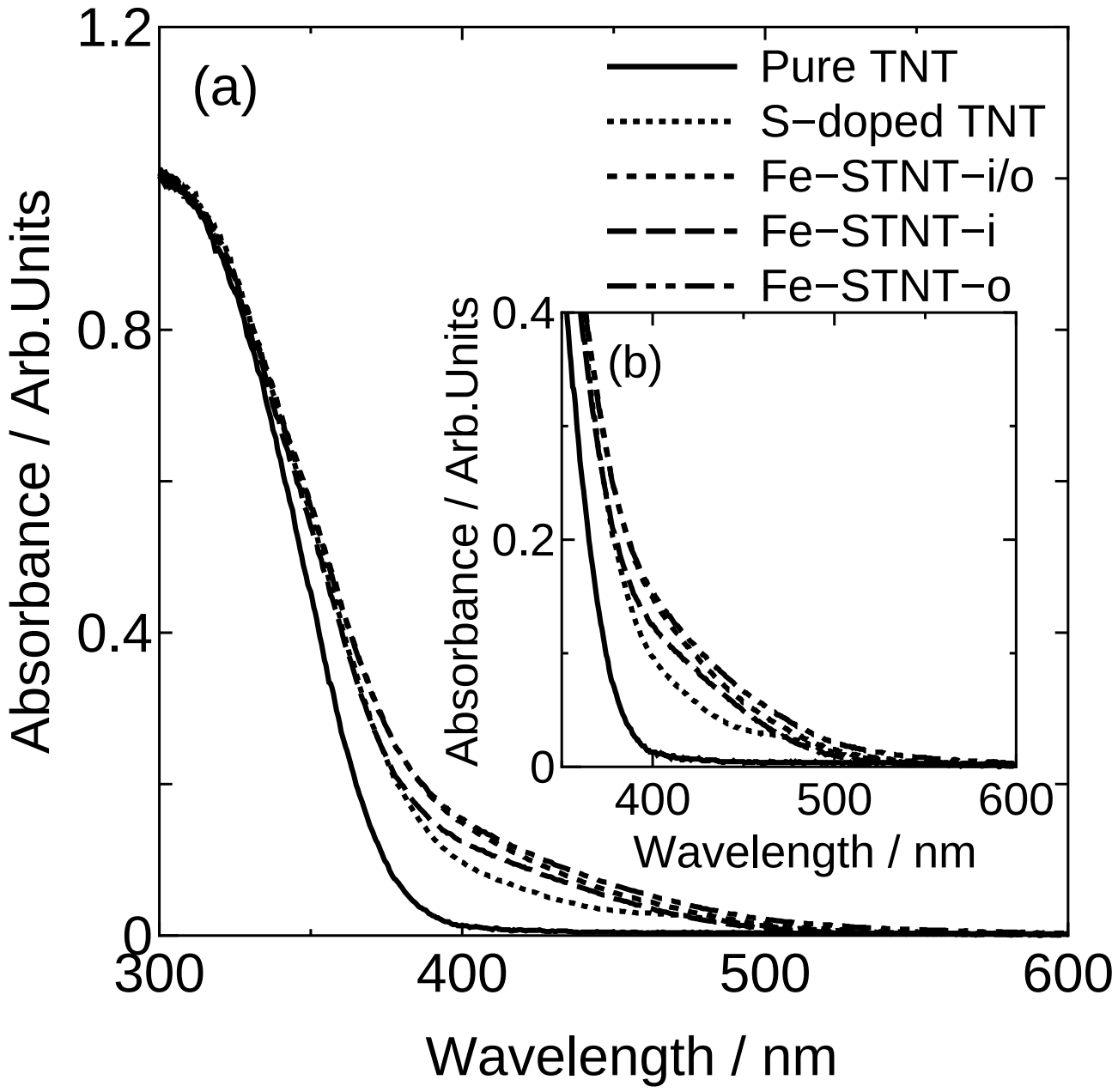
(a)
Pure TNT
S−doped TNT
Fe−STNT−i/o
Fe−STNT−i
Fe−STNT−o
Absorbance / Arb.Units
Wavelength / nm
1.2
0.8
0.4
0
300
400
500
600
(b)
0.4
0.2
0
400
500
600

figure 2

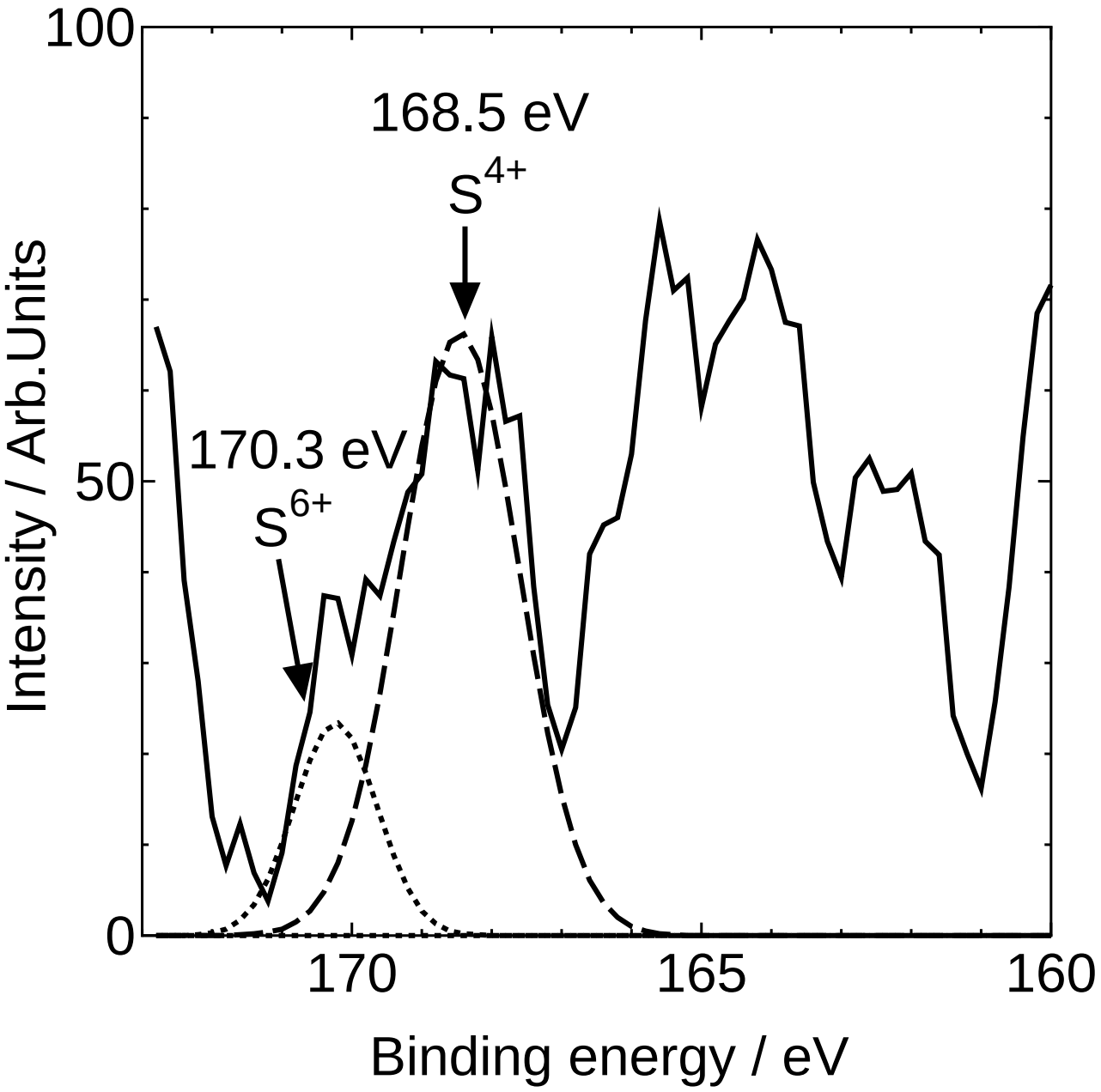
100
50
0
Intensity / Arb.Units
168.5 eV
S4+
170.3 eV
S6+
170
165
160
Binding energy / eV

figure 3

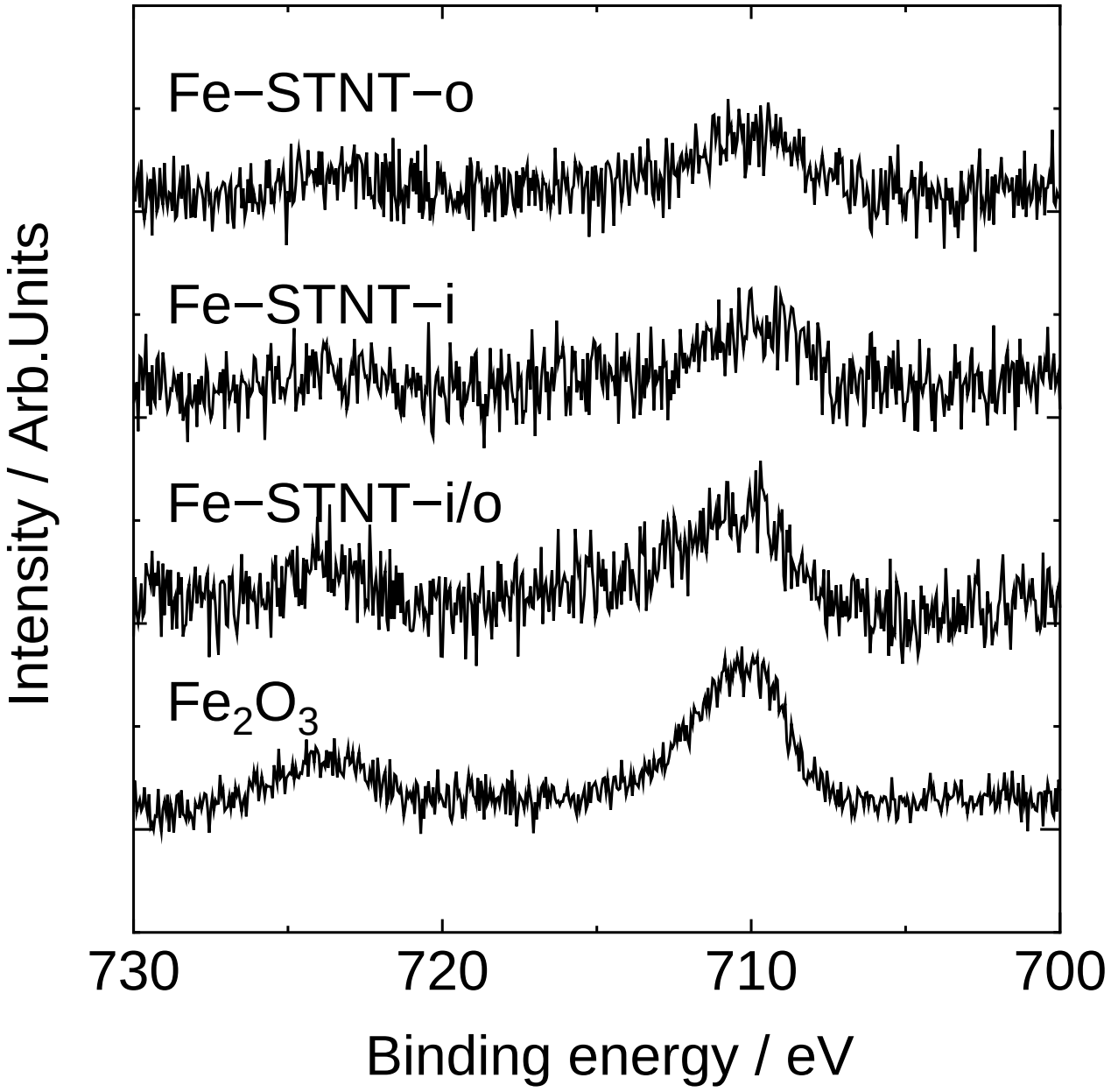
Fe−STNT−o
Fe−STNT−i
Fe−STNT−i/o
Fe2O3
Intensity / Arb.Units
730
720
710
700
Binding energy / eV

figure 4

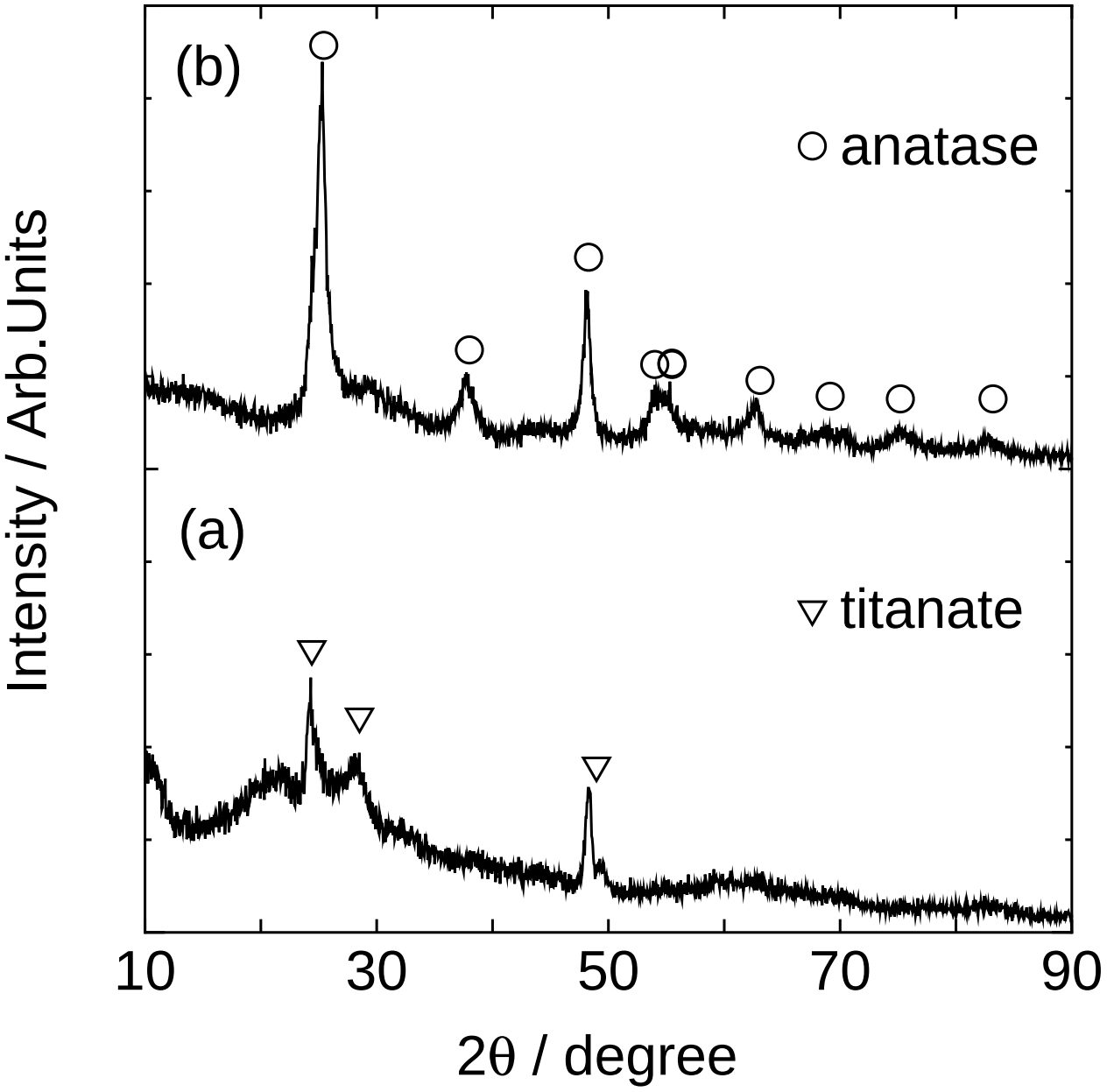
(b)
anatase
(a)
titanate
Intensity / Arb.Units
10
30
50
70
90
2θ / degree

figure 5 (a)
Click here to download high resolution image

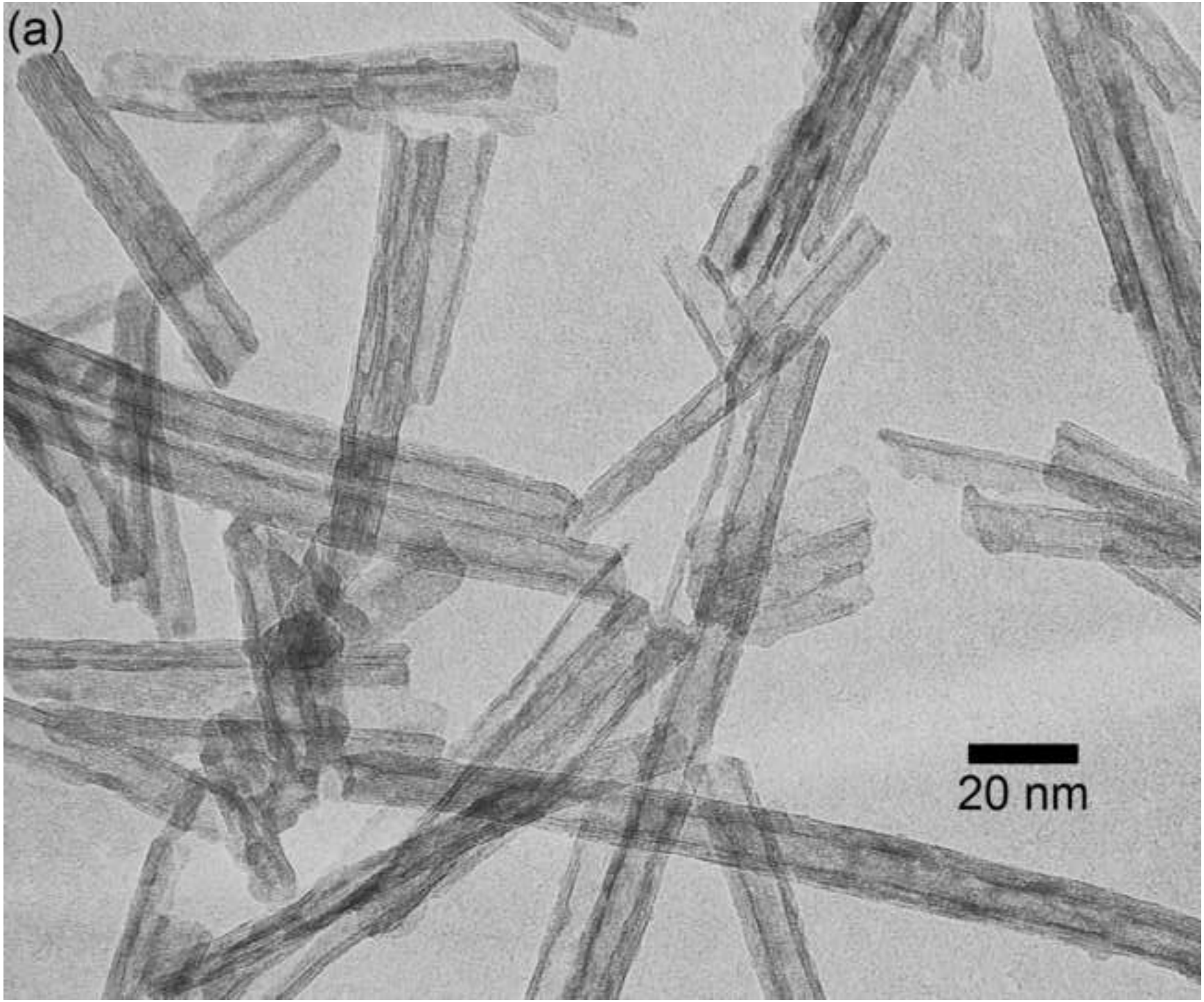

figure 5 (b)

Click here to download high resolution image

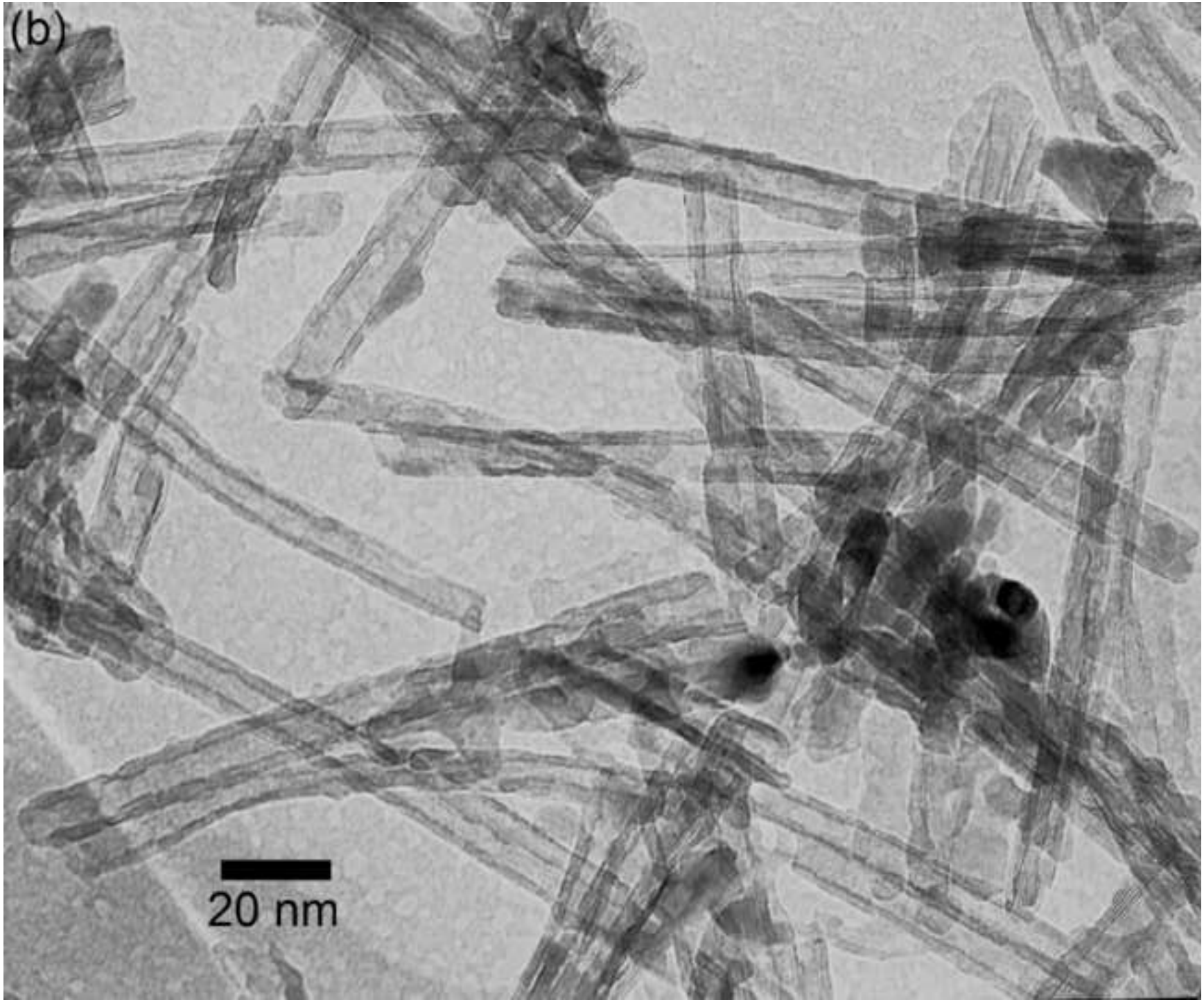

figure 6 (a)

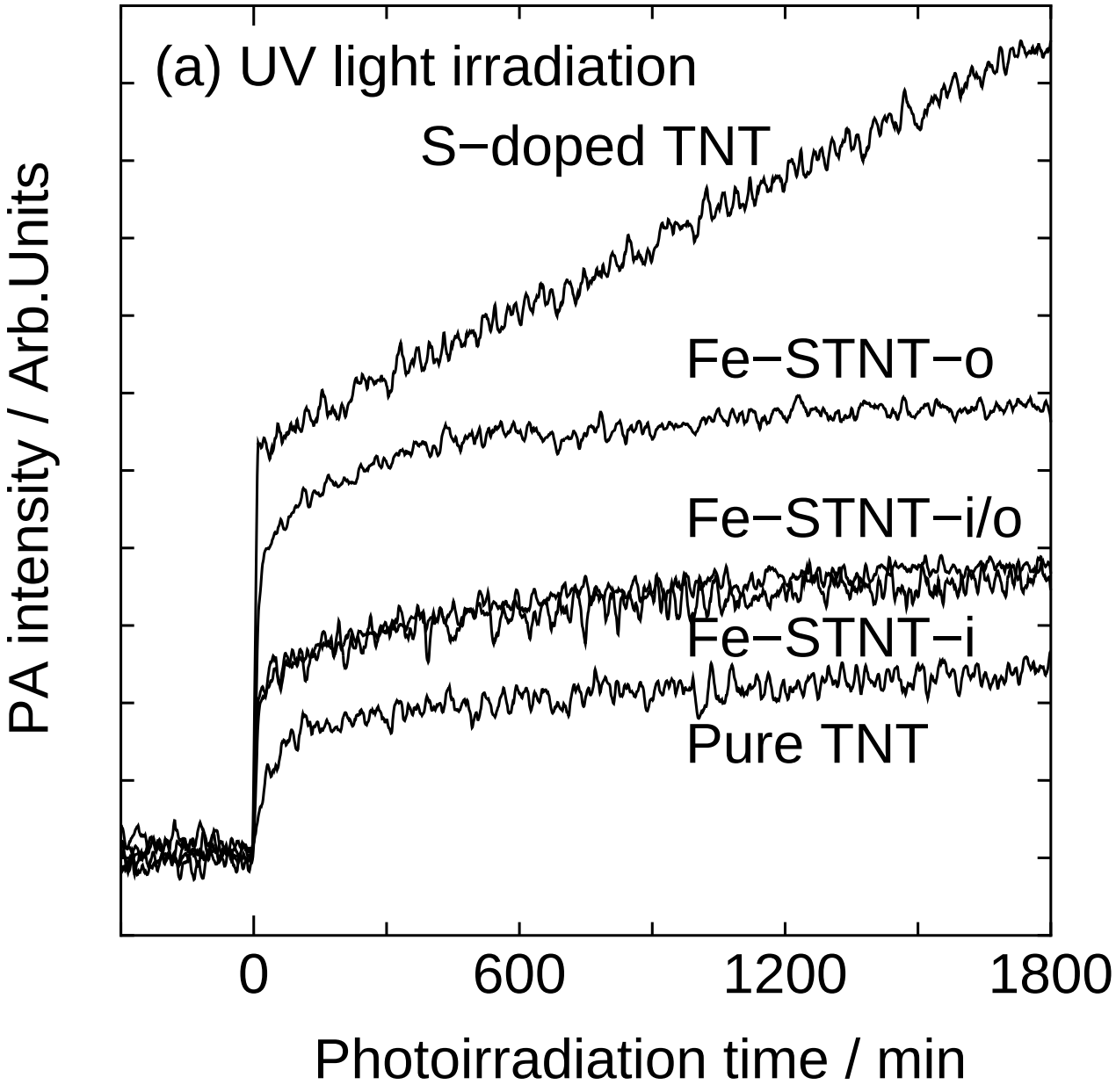
(a) UV light irradiation
S−doped TNT
Fe−STNT−o
Fe−STNT−i/o
Fe−STNT−i
Pure TNT
PA intensity / Arb.Units
0
600
1200
1800
Photoirradiation time / min

figure 6 (b)

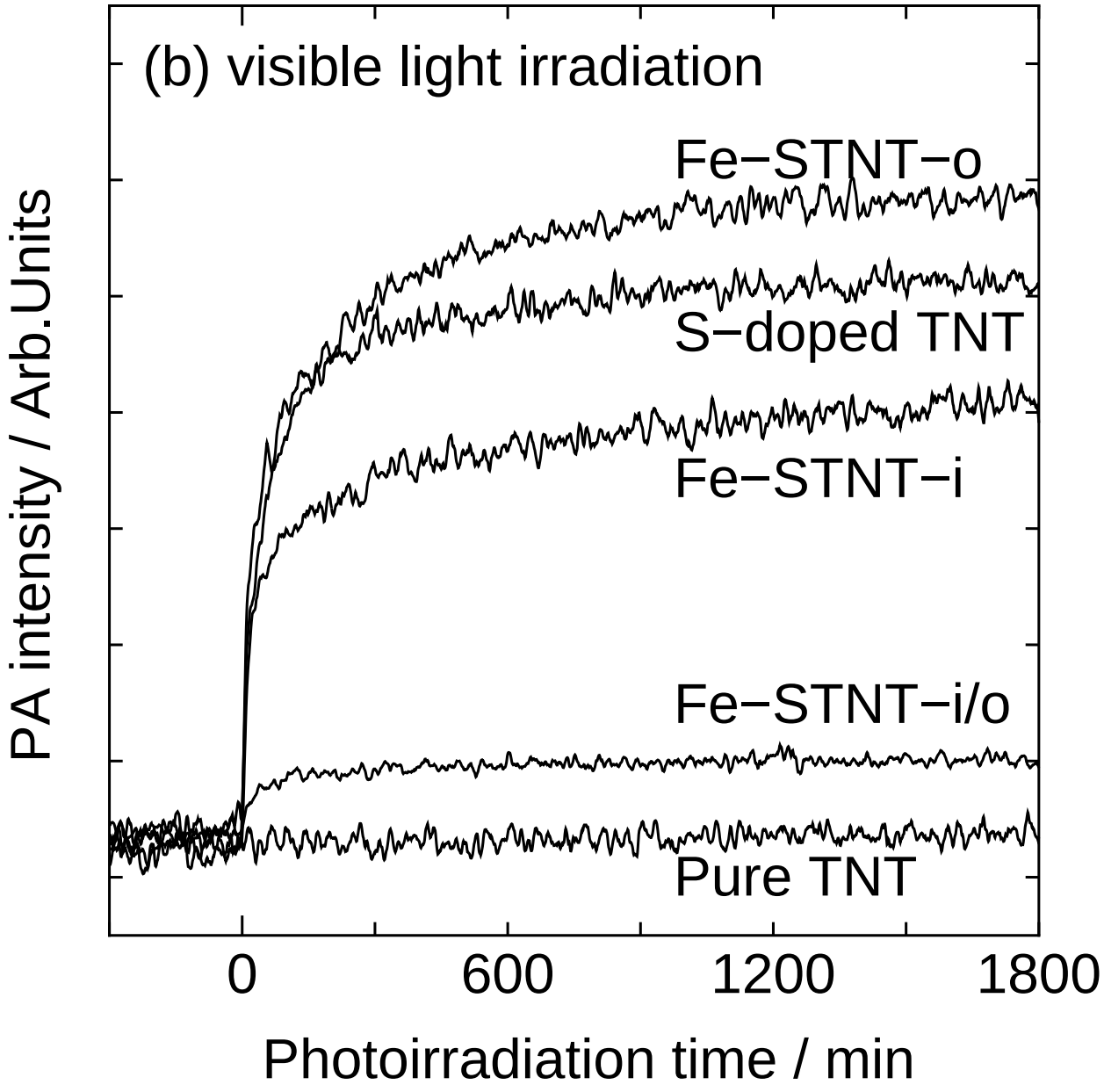
(b) visible light irradiation
Fe−STNT−o
S−doped TNT
Fe−STNT−i
Fe−STNT−i/o
Pure TNT
PA intensity / Arb.Units
0
600
1200
1800
Photoirradiation time / min

figure 7
Click here to download high resolution image

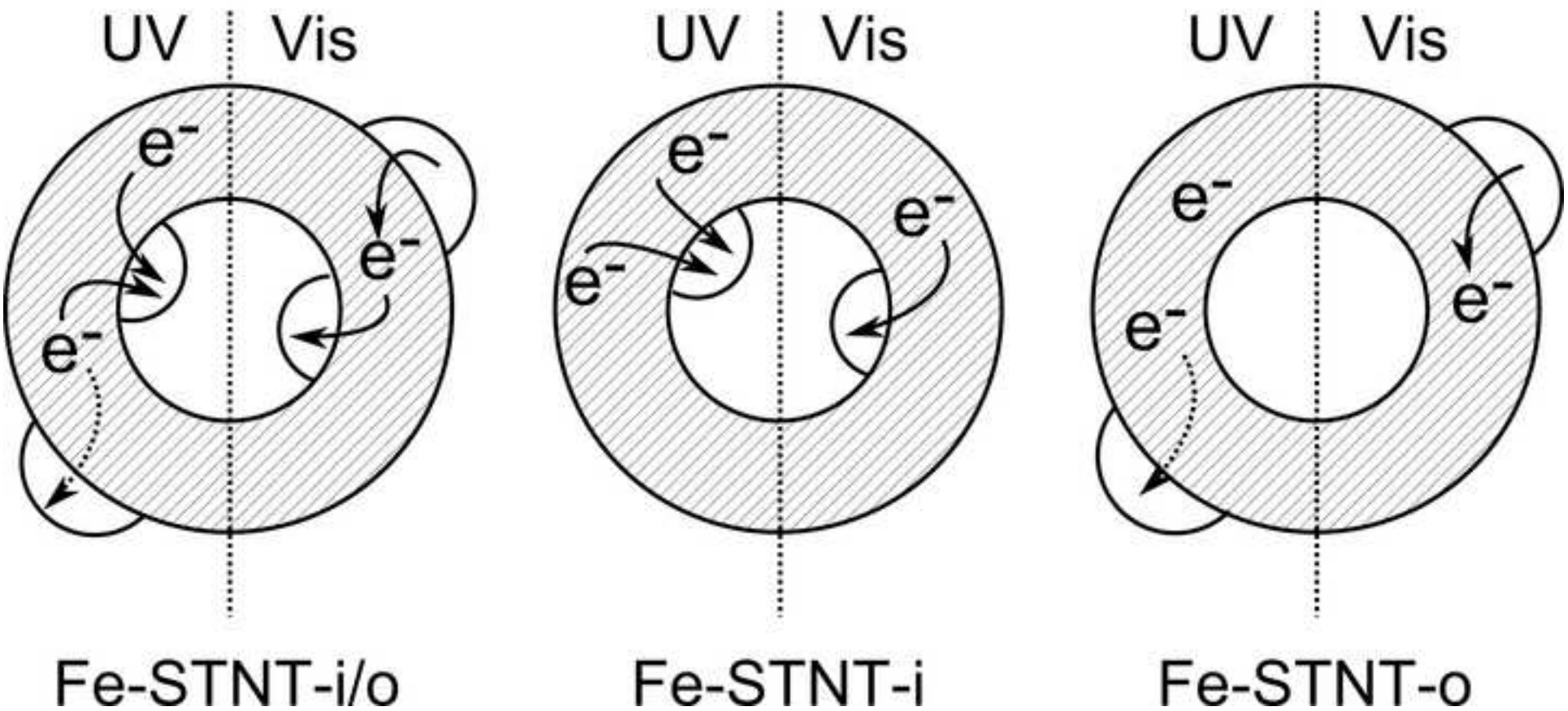

figure 8 (a)

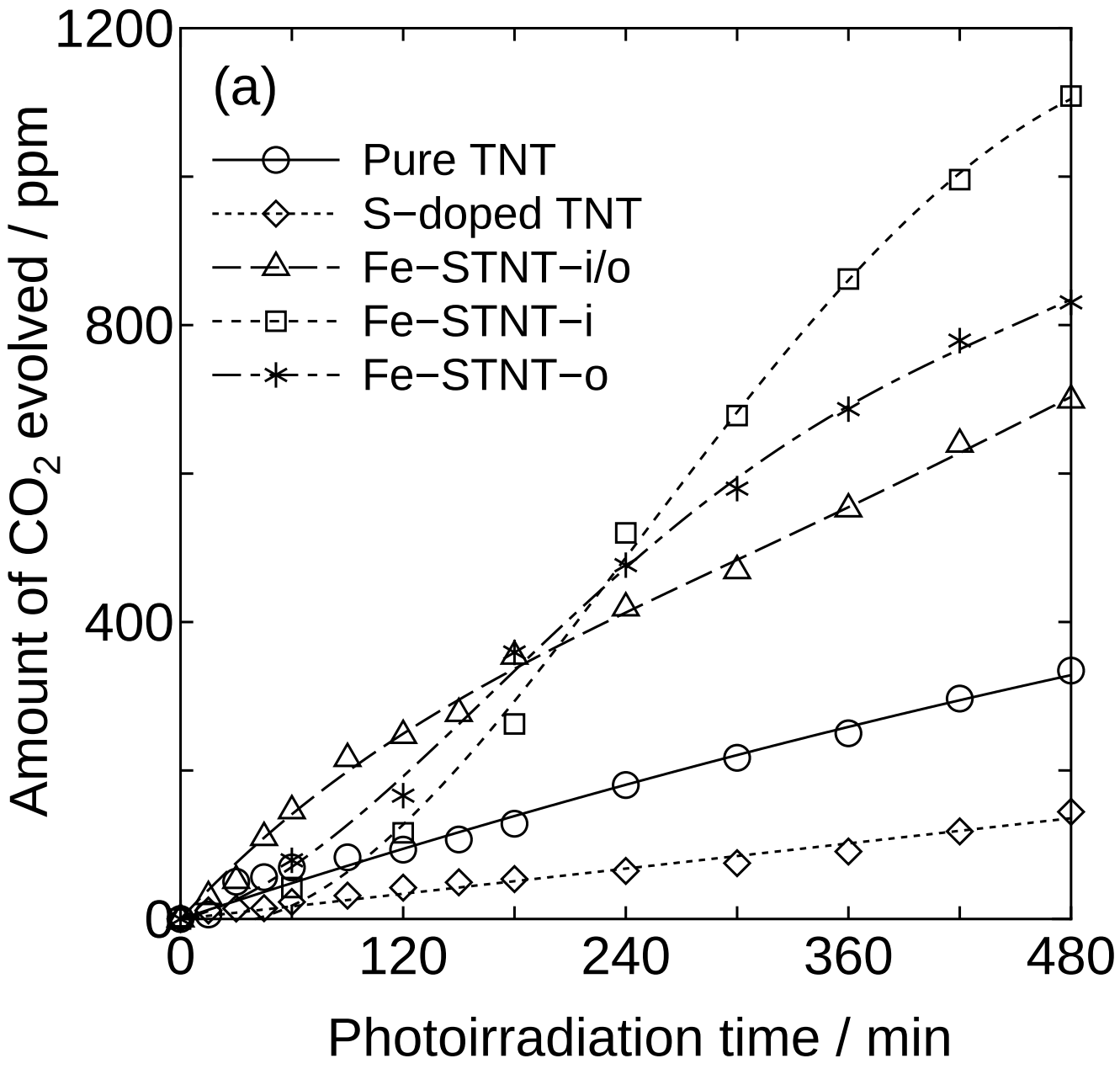
(a)
Pure TNT
S−doped TNT
Fe−STNT−i/o
Fe−STNT−i
Fe−STNT−o
Amount of CO_2 evolved / ppm
Photoirradiation time / min
0
400
800
1200
0
120
240
360
480

figure 8 (b)

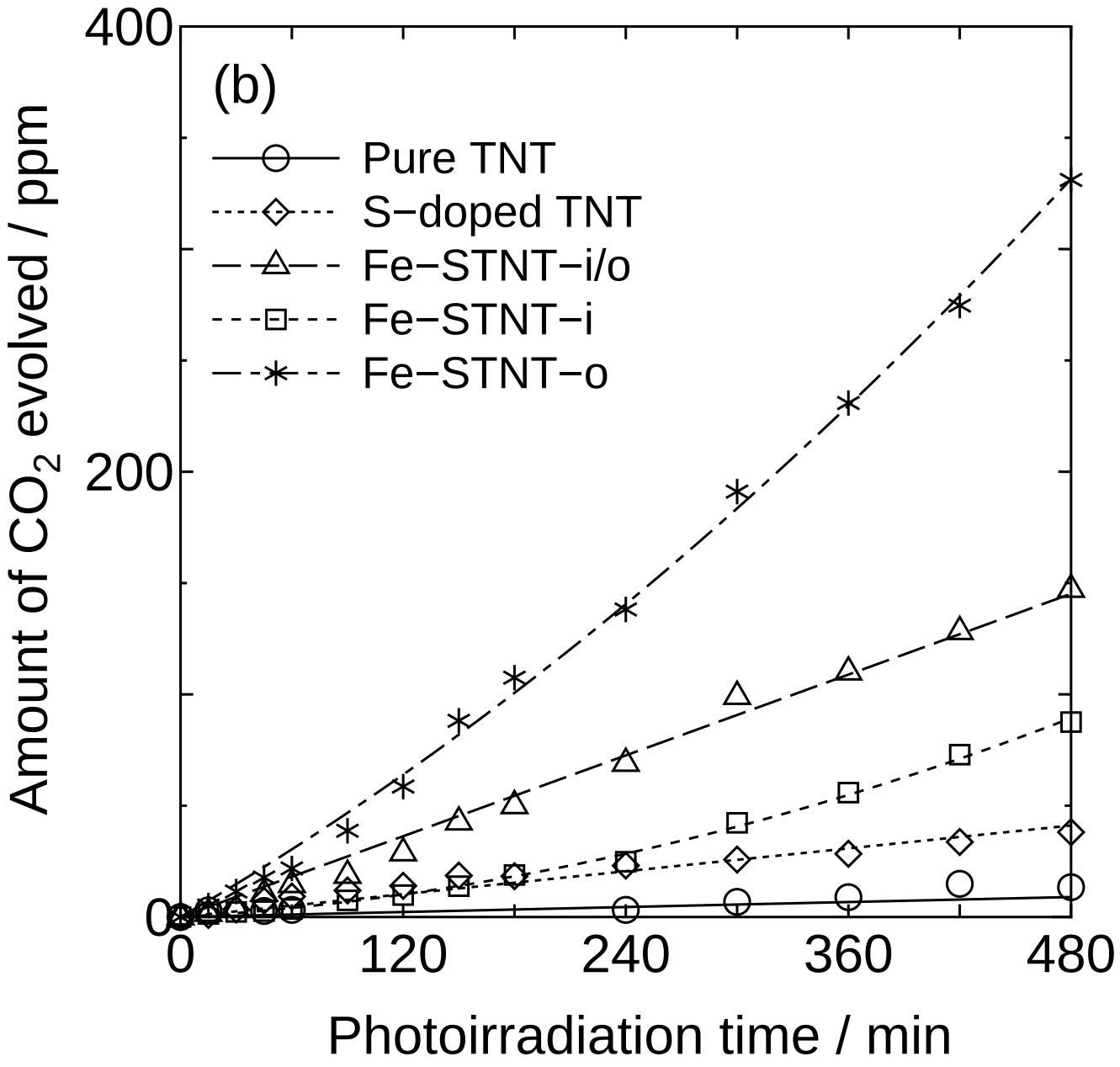
(b)
Pure TNT
S−doped TNT
Fe−STNT−i/o
Fe−STNT−i
Fe−STNT−o
Amount of CO_2 evolved / ppm
Photoirradiation time / min
0
200
400
0
120
240
360
480

figure 9

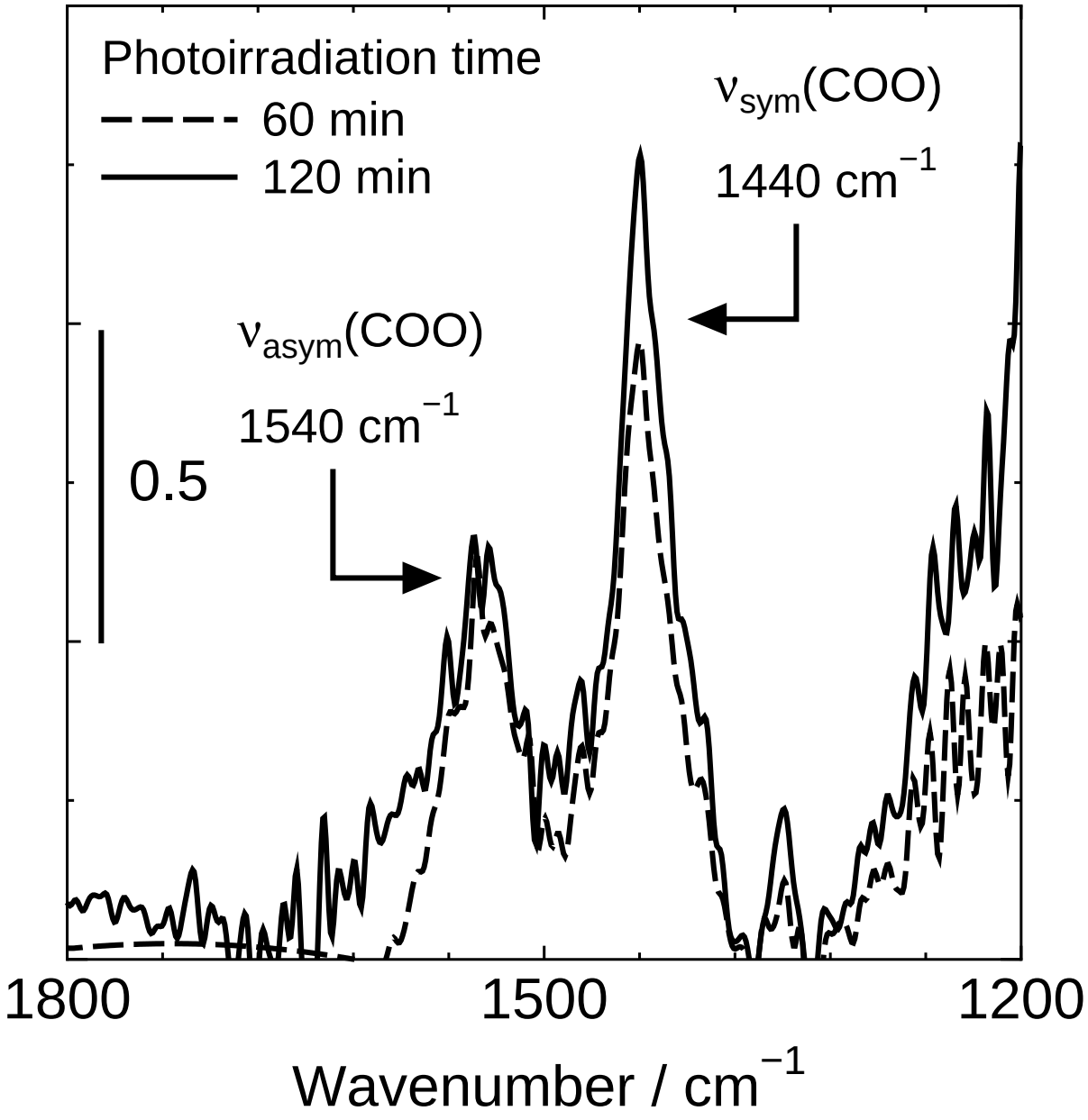
Photoirradiation time
60 min
120 min
ν_{sym}(COO)
1440 cm^{-1}
ν_{asym}(COO)
1540 cm^{-1}
0.5
1800
1500
1200
Wavenumber / cm^{-1}